

## REGULARIZED RECONSTRUCTION OF THE DIFFERENTIAL EMISSION MEASURE FROM SOLAR FLARE HARD X-RAY SPECTRA

M. PRATO

*Dipartimento di Matematica, Università di Genova, via Dodecaneso 35,  
I-16146 Genova, Italy*

M. PIANA

*Dipartimento di Informatica, Università di Verona, Ca' Vignal 2, Strada le Grazie 15,  
37134 Verona, Italy  
(e-mail: michele.piana@univr.it)*

J.C. BROWN

*Department of Physics and Astronomy, University of Glasgow, The Kelvin Building,  
G12 8QQ, U.K.*

A.G. EMSLIE

*Department of Physics, Oklahoma State University, Stillwater, OK 74078, U.S.A.*

E.P. KONTAR

*Department of Physics and Astronomy, University of Glasgow, The Kelvin Building,  
G12 8QQ, U.K.*

and

A.M. MASSONE

*CNR-INFM LAMIA, via Dodecaneso 33, I-16146 Genova, Italy*

(Received 8 July 2005; accepted 24 April 2006; Published online 11 July 2006)

**Abstract.** We address the problem of how to test whether an observed solar hard X-ray bremsstrahlung spectrum ( $I(\epsilon)$ ) is consistent with a purely thermal (locally Maxwellian) distribution of source electrons, and, if so, how to reconstruct the corresponding differential emission measure ( $\xi(T)$ ). Unlike previous analysis based on the Kramers and Bethe-Heitler approximations to the bremsstrahlung cross-section, here we use an exact (solid-angle-averaged) cross-section. We show that the problem of determining  $\xi(T)$  from measurements of  $I(\epsilon)$  involves two successive inverse problems: the first, to recover the mean source-electron flux spectrum ( $\bar{F}(E)$ ) from  $I(\epsilon)$  and the second, to recover  $\xi(T)$  from  $\bar{F}(E)$ . We discuss the highly pathological numerical properties of this second problem within the framework of the regularization theory for linear inverse problems. In particular, we show that an iterative scheme with a positivity constraint is effective in recovering  $\delta$ -like forms of  $\xi(T)$  while first-order Tikhonov regularization with boundary conditions works well in the case of power-law-like forms. Therefore, we introduce a restoration approach whereby the low-energy part of  $\bar{F}(E)$ , dominated by the thermal component, is inverted by using the iterative algorithm with positivity, while the high-energy part, dominated by the power-law component, is inverted by using first-order regularization. This approach is first tested by using simulated  $\bar{F}(E)$  derived from *a priori* known forms of  $\xi(T)$  and then applied to hard X-ray spectral data from the *Reuven Ramaty High Energy Solar Spectroscopic Imager* (RHESSI).

## 1. Introduction

Although it has long been accepted (*e.g.*, Korchak and Ponomarenko, 1965) that bremsstrahlung continuum radiation is the source of solar flare hard X-rays, it is still unclear to what extent the electron distribution responsible for the emission comprises (a) non-thermal particles trapped in a low-density plasma (thin-target), (b) particles “injected into” and stopped in a dense plasma (thick-target), (c) a spatial distribution of locally Maxwellian electrons with a location-dependent temperature ( $T$ ), or some mixture of these three situations. In all cases, however (neglecting anisotropy and albedo effects), the relationship

$$I(\epsilon) = \int_V \int_{\epsilon}^{\infty} F(E, \mathbf{r}) n(\mathbf{r}) Q(\epsilon, E) dE dV \quad (1)$$

holds, where  $I(\epsilon)$  is the bremsstrahlung emission rate (photons  $\text{s}^{-1} \text{keV}^{-1}$ ),  $n(\mathbf{r})$  ( $\text{cm}^{-3}$ ) is the plasma density,  $F(E, \mathbf{r})$  is the electron flux density spectrum (electrons  $\text{cm}^{-2} \text{s}^{-1} \text{keV}^{-1}$ ) at location  $\mathbf{r}$  in the source volume  $V$  ( $\text{cm}^3$ ), and  $Q(\epsilon, E)$  ( $\text{cm}^2 \text{keV}^{-1}$ ) is the bremsstrahlung cross-section for an electron of energy  $E$  and a photon of energy  $\epsilon$ . Under a purely thermal interpretation of Equation (1) (Brown, 1974), the electron distribution is assumed to be locally Maxwellian, *i.e.* (with  $T$  in energy units)

$$F(E, \mathbf{r}) = \frac{2^{3/2}}{(\pi m_e)^{1/2}} \frac{n(\mathbf{r}) E}{[T(\mathbf{r})]^{3/2}} e^{-E/T(\mathbf{r})}, \quad (2)$$

so that Equation (1) becomes

$$I(\epsilon) = \frac{2^{3/2}}{(\pi m_e)^{1/2}} \int_0^{\infty} \int_{\epsilon}^{\infty} n^2(T) \frac{E}{T^{3/2}} e^{-E/T} Q(\epsilon, E) dE \frac{dV}{dT} dT, \quad (3)$$

and the photon spectrum then provides information on the differential emission measure loosely defined, for stratified structures, by

$$\xi(T) = n^2(T) \frac{dV}{dT}. \quad (4)$$

A direct connection between  $I(\epsilon)$  and  $\xi(T)$  can be established by inserting expression (2) for the local electron distribution into the model-independent Equation (1), with a Kramers approximation used for  $Q(\epsilon, E)$ . Because of the extreme simplicity of the Kramers form ( $Q \propto 1/\epsilon E$ ), the result is a Laplace-transform-like integral equation relating the photon spectrum ( $I(\epsilon)$ ) directly to the differential emission measure ( $\xi(T)$ ). This equation has been studied by Piana, Brown, and Thompson (1995) in the framework of regularization theory for inverse problems and applications to high-resolution balloon data (Lin and Schwartz, 1987) have been considered. Craig and Brown (1986) noticed that an analogous approximate equation could be obtained for the more complex Bethe-Heitler form of the cross-section  $Q(\epsilon, E)$ . However, both of these use a rather coarse approximation to the true cross-section, which as well as being quite smooth, has a much more complex

analytic form (Koch and Motz, 1959). In integral inversion problems, small changes in the kernel ( $Q$  here) can result in large changes in the solution (Kato, 1980; Kress, 1989) so that results using approximate representations of  $Q$  may not be reliable.

A completely rigorous description of the thermal model requires the introduction of two integral equations. First, the (isotropic) source-averaged, effective-electron flux spectrum ( $\bar{F}(E)$ ), defined as (Brown, 1971; Brown, Emslie, and Kontar, 2003)

$$\bar{F}(E) = \frac{1}{\bar{n}V} \int_V n(\mathbf{r})F(E, \mathbf{r}) dV, \quad (5)$$

is related to the photon spectrum by means of the Volterra integral equation

$$I(\epsilon) = \bar{n}V \int_{\epsilon}^{\infty} \bar{F}(E)Q(\epsilon, E) dE, \quad (6)$$

with a fully correct form of  $Q(\epsilon, E)$ . Then, Equations (2), (4), and (5) lead to the Fredholm integral equation relationship between  $\bar{F}(E)$  and  $\xi(T)$  (Brown and Emslie, 1988)

$$\bar{F}(E) = \frac{1}{\bar{n}V} \frac{2^{3/2}E}{(\pi m_e)^{1/2}} \int_0^{\infty} \frac{\xi(T)}{T^{3/2}} e^{-E/T} dT. \quad (7)$$

The aim of the present paper is to address the following two basic questions concerning the thermal model: (1) Is the available photon spectrum ( $I(\epsilon)$ ) compatible with a thermal interpretation, *i.e.*, can the observed  $I(\epsilon)$  be fully explained by a non-negative  $\xi(T)$ ? and (2) If the answer to (1) is yes, what is the actual form of  $\xi(T)$  for that particular form of  $I(\epsilon)$ ? One way to see whether an entire  $I(\epsilon)$ , or even part of it, is compatible with a thermal model for the emission process, is to test whether the corresponding  $\bar{F}(E)$  obtained by solving Equation (6) satisfies criteria arising from Equation (7), making allowances for the data-induced noise. One such test is the ‘‘derivative test’’ for thermality found by Brown and Emslie (1988). This follows directly by differentiating Equation (7) (with both sides divided by  $E$ )  $i$  times and states that an electron spectrum ( $\bar{F}(E)$ ) is compatible with a purely-thermal interpretation if and only if the quantity  $\bar{F}(E)/E$  is ‘‘completely monotonic,’’ *i.e.* its  $i$ th derivative has sign  $(-)^i$  at all  $E$ . This approach has a technical limitation. Equation (6) can be solved by using regularization techniques (Piana, 1994; Kontar *et al.*, 2004) but derived electron spectra are affected by noise in the photon spectra used. Successive derivatives in the thermality test therefore have rapidly escalating errors due to the instability of numerical differentiation. It follows that the computation of only the first two or three orders of derivative is reliable (Emslie, Coffey, and Schwartz, 1989), with the higher- $i$  terms in the ‘‘derivative test’’ too noisy to be useful. On the other hand, we can be confident that any  $\bar{F}(E)$  clearly failing the ‘‘derivative test’’ at a high confidence level, for given noise, can be ruled out as entirely due to a thermal distribution with an everywhere non-negative  $\xi(T)$ . However, even if the  $\bar{F}(E)$  does pass the ‘‘derivative’’ test, this itself does not tell us the (non-negative) form of  $\xi(T)$  to which  $\bar{F}(E)$  corresponds. Therefore, in principle, a much more effective technique would be to solve Equation (7), where

$\bar{F}(E)$  is obtained by solving Equation (6), thus describing the  $\xi(T)$  corresponding to an observed photon spectrum: if  $\xi(T) \geq 0$  for all  $T$ , then the photon spectrum can be reliably interpreted according to a thermal model for the bremsstrahlung emission; if  $\xi(T) < 0$  for some temperature interval, then at least part of the emission is certainly non-thermal. Furthermore, the knowledge of possible features in such reconstructed form could yield important information on plasma heating and conduction processes (Brown, 1974; Brown, Melrose, and Spicer, 1979; Gabriel, 1992). In recent years, this inversion problem has achieved an unprecedented level of importance because of the high-resolution photon spectra ( $\Delta\epsilon \simeq 1$  keV) obtained from the RHESSI mission (Lin *et al.*, 2002). Combined with optimization of computational methods for regularized solutions of the ill-posed inverse problem involved (Craig and Brown, 1986; Johns and Lin, 1992; Thompson *et al.*, 1992; Piana, 1994; Piana *et al.*, 2003; Massone *et al.*, 2003; Kontar *et al.*, 2004, 2005) it is now possible to infer mean source electron spectra ( $\bar{F}(E)$ ) (see Equation (6)) with which specific physical source models can be compared (Brown, Emslie, and Kontar, 2003).

A basic technical difficulty in the reconstruction of  $\xi(T)$  is due to the fact that solving the second inverse problem (7) is extremely problematic. Simple changes of variables reduce this problem to a Laplace transform inversion problem with noisy data. There is a vast literature (Davies and Martin, 1979; Varah, 1983; Essah and Delves, 1988) showing that this problem is intrinsically highly pathological, due to the very broad filtering action of the Fredholm–Laplace integral kernel (compared to that in the basic bremsstrahlung inverse problem (6), which is of Volterra type and not severely filtering). Several regularization methods (McWhirter and Pike, 1978; Bertero, Brianzi, and Pike, 1985; Brianzi and Frontini, 1991) have been introduced to handle this inversion by reducing the unphysical oscillations due to the presence of noise. For all of them, two considerations are mandatory: first, that, as stated by Davies and Martin (1979) “[in the Laplace inversion problem with noisy data] no single method gives optimum results for all purposes...,” and therefore no general method exists which is effective at the highest level for all physical situations and all kinds of data; second, that, whatever method is applied, even with very accurate data, only a coarse resolution will be achieved in the recovered solution (Bertero, Brianzi, and Pike, 1982).

Most inversion methods for the real Laplace transform have been formulated within the framework of regularization theory for ill-posed inverse problems (Bertero, 1989). At the core of these approaches, there is the search for an optimal trade-off between stability against unphysical oscillations and accurate reproducibility of the data. Such an optimization result is obtained either by fixing a real positive regularization parameter in Tikhonov-like methods (Tikhonov, 1963) or by applying some stopping rule to iterative procedures. However, the present application is particularly challenging owing to the particular nature of the solar spectral data involved here. Typical solar  $\bar{F}(E)$  are characterized by a large dynamic range (at least three orders of magnitude for around one order of magnitude in the

$E$  range) and, more significantly, the corresponding  $\xi(T)$  have completely different forms at low and high  $T$ : at small  $T$ , a near-thermal ( $\delta$  function) component which differs from zero only in a small  $T$  range (narrow support); at high  $T$ , a monotonic component spread over a large interval. A consequence of this complexity in the source function is that regularization approaches may lose some (or most) of their effectiveness. For example, the reconstruction of  $\xi(T)$  at low  $T$  with classical Tikhonov regularization may correctly reproduce the location of the temperature peak but typically presents ringing effects whose negative components, which are numerical artefacts, might suggest that the spectrum is not thermally interpretable. Negative ringing can be eliminated by applying a reconstruction method with a positivity constraint. However, such an approach is not effective at recovering the high-temperature part of  $\xi(T)$ , which has a power-law-like behavior and requires regularization methods with more smoothing power. To deal with these kinds of difficulty, in the present paper, we utilize the following approach: an iterative scheme with a positivity constraint is applied for the inversion of the low-energy part of  $\bar{F}(E)$ , in order to eliminate unphysical ringing effects with negative oscillations in the reconstruction of the part of  $\xi(T)$  characterized by a narrow support; then, a first-order Tikhonov regularization method is applied for the inversion of the high-energy part of  $\bar{F}(E)$ , where an appropriate boundary condition constrains the reconstructed  $\xi(T)$  to behave well (*i.e.*, with a slope compatible with the spectral index of the photon data) at high  $T$ . The two reconstructed  $\xi(T)$  are then connected together noting that the connection temperature is easily determined by the  $T$  value where the thermal  $\xi(T)$  goes to zero, *i.e.* the high- $T$  limit of the narrow support of the thermal  $\xi(T)$ . We observe that, as far as the inversion of the low-energy part of  $\bar{F}(E)$  is concerned, the use of the positivity constraint in the inversion makes the thermality test based on the verification that the reconstructed  $\xi(T)$  is positive at all  $T$ , inappropriate, since positivity is forcefully imposed in the inversion procedure. Therefore, for this inverse problem, the compatibility between the data and the thermal model is tested by checking whether the residuals in  $\bar{F}(E)$  corresponding to the  $\xi(T)$  recovered by exploiting the positivity constraint are statistically acceptable.

The plan of the paper is as follows. In Section 2 the regularization methods for the reduction of the numerical instability of the problem are introduced. In Section 3, we test these regularization approaches in some significant synthetic cases. Section 4 applies the method to actual RHESSI photon spectra, and our conclusions are offered in Section 5.

## 2. Regularization Methods

We could in principle proceed directly from Equation (7) to see whether some  $\bar{F}(E)$  could be wholly thermal in origin if we had a completely reliable inversion method: given a data vector  $\bar{F}(E)$ , a wholly thermal interpretation of it is possible if and only if the  $\xi(T)$  obtained by the inversion method has no statistically significant

negative values over any range of temperature ( $T$ ). Our aim here is to address this problem by means of two numerical algorithms based on regularization theory for ill-posed inverse problems, keeping in mind that the effectiveness of any regularized inversion approach in the present case is much weaker than for most other linear inverse problems due to the extreme numerical instability of the Laplace problem, with its very broad kernel. A quantitative estimate (Golub and van Loan, 1996) for the instability of linear equations like Equation (7) is given in terms of the condition number ( $C$ ) of the kernel (cross-section) matrix by

$$\Delta_{\text{solution}} \leq C \Delta_{\text{data}}, \quad (8)$$

where  $\Delta_{\text{data}}$  is a norm of the relative error on the data and  $\Delta_{\text{solution}}$  is a compatible norm of the propagated relative error on the solution. It can be shown (Craig and Brown, 1986, Table 7.1; Piana, Brown, and Thompson, 1995) that, for typical solar data parameters, the condition number associated with the (Fredholm) Equation (7) is of the order of  $10^{10}$ , which is much bigger, for similar parameters than the condition number, around  $10^3$ , associated with the (Volterra) bremsstrahlung spectrum to electron spectrum inversion problem (6) (Piana and Brown, 1998). The actual consequences of ill-conditioning are highly significant. A regularization algorithm essentially expresses the approximate smoothed solution as a truncated linear sum of some basis functions. In the basic bremsstrahlung spectrum inversion problem Equation (6),  $\bar{F}(E)$  can be expressed in terms of around ten basis functions for typical noise in the case of a data vector with around 100 points, while in the differential emission measure inversion problem (Equation (7)) we find that only two, or at most three, basis functions can be meaningfully included in the expansion of  $\xi(T)$ . Therefore, in the recovery of  $\xi(T)$  it is necessary to introduce much more severe constraints than the one adopted in the  $\bar{F}(E)$  inversion procedure described, for example, in Piana *et al.* (2003). Even incorporating these constraints, it will be impossible to achieve a temperature resolution anywhere nearly comparable with the spectral resolution with which  $\bar{F}(E)$  can be reconstructed through the solution of the bremsstrahlung Equation (6) (*cf.* the analysis of the temperature resolution problem in Craig and Brown, 1986, pp. 100–120).

Adopting the change of variable  $y = 1/T$ , Equation (7) becomes

$$K \frac{\bar{n}V\bar{F}(E)}{E} = \int_0^\infty f(y) \exp(-Ey) dy, \quad (9)$$

where  $K = \sqrt{\pi m_e/8} = 1.89 \times 10^{-14} \text{ gm}^{1/2} = 4.73 \times 10^{-10} \text{ keV}^{1/2} \text{ cm}^{-1} \text{ s}$  and  $f(y)$  ( $\text{cm}^{-3} \text{ keV}^{-1/2}$ ) is defined as

$$f(y) = \frac{\xi(1/y)}{y^{1/2}}, \quad (10)$$

with  $\xi(T)$  in units of  $\text{cm}^{-3} \text{ keV}^{-1}$ . Equation (9) involves a continuous representation of the model ( $f(y)$ ) and of the data ( $\bar{F}(E)$ ), while real data are discrete, truncated,

and affected by measurement and systematic noise. In reality, therefore, the situation is described by the (finite rank linear) operator  $L: X \rightarrow Y$  such that

$$(Lf)_n = \int_0^\infty f(y) \exp(-E_n y) dy, \quad n = 1, \dots, N, \quad (11)$$

where the  $\{E_n\}_{n=1}^N$  are the sampled electron energies,  $X$  is the functional space containing the solution, and  $Y$  the Euclidean space containing the data. Then our problem is to solve

$$Lf = \mathbf{g}, \quad (12)$$

with data vector  $\mathbf{g}$  in  $Y$  having components

$$g_n = K \frac{\bar{n} V \bar{F}(E_n)}{E_n}, \quad n = 1, \dots, N. \quad (13)$$

As already stated, Equation (12) is a strongly ill-conditioned linear problem and the only way to obtain a realistic approximate solution in the presence of noise is some reconstruction technique based on regularization theory for linear inverse problems. One approach is the first-order Tikhonov method (Tikhonov, 1963; Craig and Brown, 1986), which solves the minimization over  $f$  of

$$\|Lf - \mathbf{g}\|_Y^2 + \lambda \|f'\|_X^2 = \text{minimum}, \quad (14)$$

where  $\lambda$  is the (real positive) regularization parameter. It can be proved (Piana, Brown, and Thompson, 1995) that under boundary conditions

$$f(0) = 0 \quad (15)$$

and

$$\lim_{y \rightarrow \infty} f'(y) = 0 \quad (16)$$

the analytical solution of Equation (14) is

$$f_\lambda(y) = \sum_{k=1}^N \frac{\sigma_k}{\sigma_k^2 + \lambda} (\mathbf{g}, \mathbf{v}_k)_Y u_k(y), \quad (17)$$

where the  $\sigma_k$  and  $\mathbf{v}_k$  are respectively the eigenvalues and eigenvectors of the matrix

$$G_{nm} = \int_0^\infty \phi'_n(y) \phi'_m(y) dy, \quad (18)$$

$$\phi_n(y) = \frac{1}{E_n^2} (1 - e^{-E_n y}) \quad (19)$$

and

$$u_k(y) = \frac{1}{\sigma_k} \sum_{n=1}^N (\mathbf{v}_k)_n \phi_n(y). \quad (20)$$

For this problem, first-order regularization is more effective than zero-order regularization for two basic reasons. First of all, it prescribes a bound on the first derivative of the regularized solution which, in this case of large numerical oscillations, is a sensible thing to do. Second, in this particular implementation, condition (15) constrains the regularized solution to behave well at  $y = 0$  ( $T \rightarrow \infty$ ), thus improving the restoration accuracy for  $\xi(T)$  at high  $T$ . It is also true, however, that condition (16) has no physical basis, and hence may yield artefacts at low  $T$ .

The main disadvantage of using Tikhonov regularization is that solutions with negative components can result from noisy data. In particular, in the reconstruction of the low-temperature component of  $\xi(T)$ , typically characterized by a very narrow support, an effective method would allow us to constrain the restored solution to be positive, thus avoiding unphysical ringing effects due to the presence of noise on the data. The introduction of such a constraint (Piana and Bertero, 1996) has the effect of increasing the resolution power of the inversion approach, allowing reconstruction of more details in the source function. The method with positivity applied in this paper is the projected-Landweber method, first formulated by Legendijk, Biemond, and Boekee (1988) for the image restoration problem. The mathematical properties of this method are discussed, for example, by Eicke (1992) and an accelerated version has been provided by Piana and Bertero (1997). We first consider the discretized version of Equation (12)

$$\mathbf{g} = \mathbf{L}\mathbf{f} \quad (21)$$

where  $\mathbf{f}$  comes from the sampling of (10) and  $\mathbf{L}$  is the matrix with entries

$$L_{mn} = \exp(-E_n y_m) \delta y \quad (22)$$

where the  $y_m$ ,  $m = 1, \dots, M$  are uniformly sampled and  $\delta y$  is an appropriate integration weight. The projected-Landweber method provides reconstructions of  $f(y)$  (and therefore of  $\xi[T]$ ) by optimally stopping the iteration

$$\mathbf{f}_{k+1} = P_+(\mathbf{f}_k + \tau \mathbf{L}^T(\mathbf{g} - \mathbf{L}\mathbf{f}_k)), \quad \mathbf{f}_0 = 0, \quad (23)$$

where  $\tau$  is a relaxation parameter,  $\mathbf{L}^T$  is the transpose matrix of  $\mathbf{L}$ , and  $P_+$  sets to zero all the negative components at each iteration.

As already stated in Section 1, the regularization effects on the approximate solutions provided by Tikhonov first-order regularization and by the projected-Landweber method can be obtained by fixing  $\lambda$  in Equation (17) and the iteration number in Equation (23). To this purpose, many criteria have been introduced (Davies, 1992); here we adopted the same approach as in Piana *et al.* (2003), based on the analysis of the regularized cumulative residuals. For example, in the case of first-order Tikhonov method, we consider the function

$$S^\lambda(k) = \frac{1}{k} \sum_{i=1}^k r_i^\lambda, \quad k = 1, \dots, N \quad (24)$$

where  $r_i^\lambda$  is the  $i$ th normalized regularized residual corresponding to the regularized  $\xi(T)$ . For completely uncorrelated noise, the normalized cumulative residuals exhibit a random walk with expected deviation  $1/\sqrt{k}$ . In Equation (24), the presence of the regularization parameter increasingly correlates the  $r_i^\lambda$  for increasing values of  $\lambda$ . Therefore, an optimal criterion to fix  $\lambda$  is to look for the largest value of  $\lambda$  such that  $|S^\lambda(k)|$  is bounded by  $3/\sqrt{k}$ . An analogous procedure is followed for stopping the projected iterations, whereby, in this case, the regularization parameter is represented by the iteration number.

### 3. Simulations

In this section, we wish to test the effectiveness of the regularization approach as introduced in the previous section. In particular, in Section 3.1 we describe the case of a power law with a low-energy cutoff showing that if the mean electron spectrum is sampled starting from energies greater than the cutoff, the reconstruction is rather accurate (in fact, the problem becomes that of recovering a pure power law in a limited domain), while the reconstruction dramatically fails if the minimum sampled energy is smaller than the energy cutoff, in accordance with the fact that a power law with a low-energy cutoff is *not* compatible with thermal bremsstrahlung emission. Then, in Section 3.2, the temperature resolution achievable by the method is discussed, in Section 3.3, the performance of the method in reconstructing power laws is tested and, finally, in Section 3.4, a realistic form of  $\bar{F}(E)$  obtained by regularized inversion of a synthetic photon spectrum is considered.

#### 3.1. COMPATIBILITY TEST

We want to verify whether an  $\bar{F}(E)$  reconstructed from photon data ( $I(\epsilon)$ ) can be interpreted as consistent with a purely thermal model. The ‘‘derivative test’’ of Brown and Emslie (1988) provides a possible approach, but does not yield information on the temperature structure of the source. A more informative approach is to apply a reconstruction method and to check if the reconstructed  $\xi(T)$  is non-negative for all  $T$ . As an example, let us consider the case of a mean source electron spectrum

$$\bar{F}(E) \propto \begin{cases} E^{-\delta} & E \geq E_c \\ 0 & E < E_c, \end{cases} \quad (25)$$

with  $E_c$  a low-energy cutoff. Before performing the inversion, however, we discuss some informative analytic aspects of Equation (25) in relation to the general expression Equation (7) for  $\bar{F}(E)$  from a purely thermal source, which we rewrite, ignoring constant factors, as

$$\bar{F}(E) \propto E \int_0^\infty \frac{\xi(T)}{T^{3/2}} e^{-E/T} dT. \quad (26)$$

First it is obvious that if  $\xi(T)$  is greater than zero over any  $T$  interval then the corresponding  $\bar{F}(E)$  is never zero at any  $E$ . Thus, the  $\bar{F}(E)$  in Equation (25) cannot be purely thermal (it clearly fails the derivative test at  $E = E_c$ ). Second, we note that for a pure power law,  $\xi(T) \propto T^{-\alpha}$  at all  $T$  with  $\alpha$  constant, the resulting  $\bar{F}(E)$  is proportional to  $E^{-\alpha+\frac{1}{2}}$  at all  $E$ . Consequently, for  $\alpha = \delta + \frac{1}{2}$  a pure (untruncated) power law  $\xi(T)$  predicts  $\bar{F}(E)$  in Equation (25) perfectly in the range  $E \geq E_c$  but completely contradicts it in the range  $E < E_c$ . Thus, a thorough thermality test must be applied to all  $E$ ; failure (within the allowed uncertainties) at even one value of  $E$  is enough to rule out a purely thermal model.

A somewhat surprising result here is that a wholly-thermal model is ruled out by the form of  $\bar{F}(E)$  at low rather than at high energies. We also emphasize that the power law relation between  $\xi(T)$  and  $\bar{F}(E)$  only holds (at  $E \geq E_c$ ) for a complete power law  $\xi(T)$ . If  $\xi(T)$  is only a power law over some finite range, say  $(T_1, T_2)$ , the corresponding  $\bar{F}(E)$  is not a power law at any  $E$  but rather, with  $x = T/E$ ,

$$\bar{F}(E) \propto E^{-\alpha+1/2} \int_{T_1/E}^{T_2/E} x^{-\alpha-3/2} e^{-1/x} dx. \quad (27)$$

We now show that application of our inversion method to data Equation (25) agrees well with these analytic results.

For the inversion, the data (25) is discretized according to uniform sampling starting from a minimum sampled energy ( $E_{\min}$ ), realistic Poisson noise is added to the corresponding photon spectrum and errors on  $\bar{F}(E)$  are generated by inverting the noisy  $I(\epsilon)$ . We applied the first-order Tikhonov inversion method for two possible experimental situations concerning the relative values of the pair  $E_c, E_{\min}$ , and for  $\delta = 2$  with the results shown in Figure 1. When  $E_c \leq E_{\min}$  (*i.e.*, the cutoff is not sampled), a stable differential emission measure is restored. There are some slight, long-wavelength oscillations in the recovered  $\xi(T)$  of roughly the width of the kernel but the mean temperature spectral index is close to the theoretical value  $\alpha = 2.5$ . On the other hand, when  $E_{\min} < E_c$  (and so the cutoff *is* sampled), the reconstruction contains large negative ranges and is absolutely unphysical as expected. This behavior is consistent with the fact that a mean source electron spectrum with any cutoff is incompatible with a purely thermal interpretation of the emission (since any Maxwellian contains electrons of all  $E$ ).

### 3.2. TEMPERATURE RESOLUTION

Heuristically, the effective temperature resolution achievable by our inversion method can be assessed by reconstructing  $\xi(T)$  forms using the  $\bar{F}(E)$  corresponding to input  $\delta$  functions  $\xi(T) \approx \delta(T - T_0)$ . The resulting reconstructed forms of  $\xi(T)$  are characterized by finite full widths at half maximum (FWHM), which estimate the resolution achievable around  $T = T_0$ . Therefore, for inverse problems the resolution power depends on the reconstruction method. In Table I, the FWHM

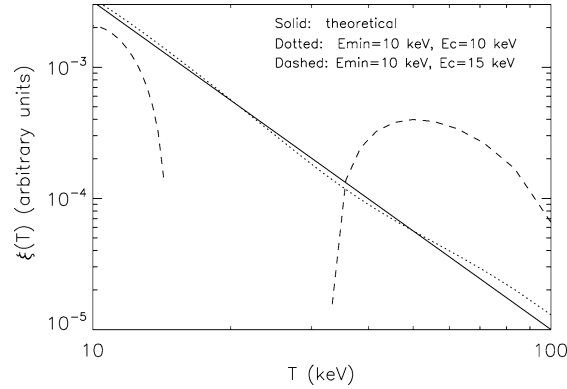


Figure 1. Reconstruction of the differential emission measure corresponding to an electron spectrum in the form of a power law with a low-energy cutoff, for two different values of the cutoff energy ( $E_c$ ) and of the minimum sampled energy ( $E_{\min}$ ). The reconstruction method is first-order Tikhonov regularization with boundary conditions. If  $E_{\min} \geq E_c$ , the sampled electron spectrum does not include a cutoff and  $\xi(T)$  is faithfully recovered (dotted line). If  $E_{\min} < E_c$ , the sampled electron spectrum does include a cutoff and so is not compatible with a thermal interpretation. In this case, the reconstruction of  $\xi(T)$  is unphysical (dashed line). The solid line is proportional to  $T^{-5/2}$  in the range 10–100 keV.

values realized through application of the two reconstruction methods discussed in Section 2 to  $\bar{F}(E)$  spectra are given for different values of  $T_0$ . The averaged electron spectra are obtained by inverting the corresponding photon spectra (affected by realistic Poisson noise) and contain 50 points in the energy range 1–50 keV.

TABLE I

Full widths at half maximum (FWHM) for the reconstruction of  $\delta$  functions peaked at different temperatures. The maximum and the centroid values of  $T$  corresponding to the reconstructed  $\xi(T)$  are also given. The inversion methods are first-order regularization with boundary conditions and projected-Landweber method with positivity.

Input ( $T_0$ , keV)	$T_{\max}$ (Tikhonov)	$\langle T \rangle$ (Tikhonov)	FWHM (Tikhonov)	$T_{\max}$ (positivity)	$\langle T \rangle$ (positivity)	FWHM (positivity)
2.5	2.3	2.6	1.5	2.5	2.5	0.8
3.5	2.8	3.3	2.0	3.6	3.6	0.9
4.5	3.4	4.6	3.3	4.6	4.6	1.1
5.5	3.9	5.7	4.2	5.6	5.6	0.9
6.5	4.5	7.1	5.6	6.6	6.6	1.5
7.5	5.2	8.5	7.3	7.6	7.6	1.3
8.5	6.1	9.0	9.4	8.3	8.5	2.6
9.5	7.3	9.6	11.8	9.6	9.7	2.3
10.5	7.9	10.5	12.3	10.6	10.8	2.3
11.5	8.6	11.6	13.2	11.6	11.6	2.4

Table I also contains values for the ‘‘centroid’’ temperature of the reconstructed distributions, defined by  $\langle T \rangle = \int T \xi(T) dT / \int \xi(T) dT$ . In the case of first-order regularization, these  $\langle T \rangle$  are 10% or so higher than the  $T_{\max}$  at which the recovered  $\xi(T)$  peaks because the  $\xi(T)$  are skewed, and they compare well with the single input  $T_0$  of the originally-assumed  $\delta$  functions. In the case of the iterative projected-Landweber method,  $\langle T \rangle$  and  $T_{\max}$  coincide in most cases and are very close to the theoretical  $T_0$ .

When first-order regularization is applied in the case of multi-thermal sources, the FWHM values given in Table I may be overly optimistic estimates of the temperature resolution particularly when trying to separate narrow features. As an example, we consider reconstructions of two  $\delta$  functions with both methods, where the first is peaked at  $T_1 = 2.5$  keV and the second is peaked at  $T_2 = 10, 7, 5, 4.5$  keV, respectively – see Figure 2. Also in this case, for the reconstruction, we considered  $\bar{F}(E)$  sampled in the energy range 1–50 keV. We note that the use of

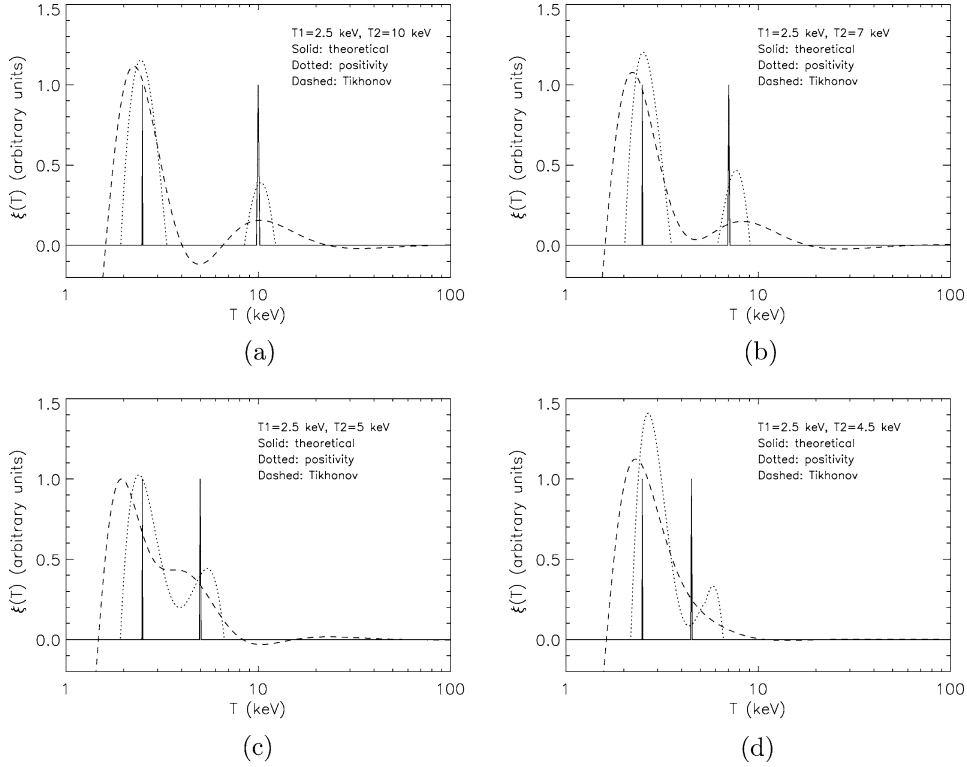


Figure 2. Reconstructions of two  $\delta$  functions (solid line) by means of first-order regularization (dashed) and projected-Landweber method (dotted). The averaged electron spectrum contains 50 points uniformly sampled in the range 1–50 keV and is obtained by inverting the corresponding photon spectrum with realistic Poisson noise added: (a)  $T_1 = 2.5$  keV,  $T_2 = 10$  keV; (b)  $T_1 = 2.5$  keV,  $T_2 = 7$  keV; (c)  $T_1 = 2.5$  keV,  $T_2 = 5$  keV; (d)  $T_1 = 2.5$  keV,  $T_2 = 4.5$  keV.

the positivity constraint increases the resolution limit as explained for example in Piana and Bertero (1996) by means of arguments based on the analytic continuation principle. Furthermore, the  $\xi(T)$  reconstructed by means of the Tikhonov method have unphysical negative components. We conclude that for the recovery of the low-temperature part of the differential emission measure, the projected algorithm is significantly more effective. We also observe that the energy range 1–50 keV, where  $\bar{F}(E)$  was sampled for this inversion, is in some sense optimal, since it always includes the peak temperatures to be recovered. In real  $\bar{F}(E)$ , energies up to typically ten keV must be avoided owing to the presence of (or problematical correction for) lines of non-bremsstrahlung origin or to systematic errors introduced by the hardware. In other words, a typical experimental situation is that  $\bar{F}(E)$  is inverted from electron energies greater than the temperatures involved in the thermal process. In order to study the effect of this on the inversion method, we considered the test shown in Figure 3. The electron spectrum corresponding to an isothermal  $\xi(T)$  with  $T_0 =$  seven keV is inverted for different electron energy sampling ranges: 2–20 keV (solid), 2–7 keV (dashed), 7–20 keV (dotted), and 20–70 keV (dot-dashed). We found that if  $T_0$  is higher than the energy range considered, the reconstruction preserves the symmetry of the  $\delta$  function (so that  $T_{\max}$  and  $\langle T \rangle$  more or less coincide) but the peak temperature is notably overestimated (almost 20%). If  $T_0$  is smaller than the sampled energies (which is the realistic situation), the reconstruction is rather skewed (in such a way that  $T_{\max}$  is bigger than  $\langle T \rangle$ , as opposed to the case of Tikhonov regularization), presents a widened FWHM and the peak temperature is slightly underestimated: for example, if the selected range is 20–70 keV, the reconstructed  $T_{\max}$  is  $\approx 5\%$  smaller than the true one.

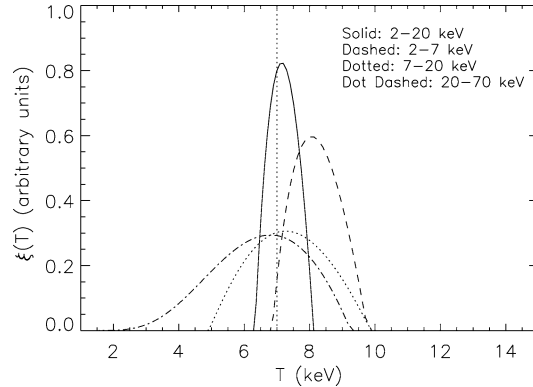


Figure 3. Reconstruction of a  $\delta$  function peaked at  $T_0 =$  seven keV when the corresponding  $\bar{F}(E)$  is sampled over different electron energy ranges: 2–20 keV (solid); 2–7 keV (dashed); 7–20 keV (dotted); 20–70 keV (dot-dashed). The reconstruction method is the projected-Landweber method with positivity.

### 3.3. POWER LAWS

The situation is notably different for the recovery of the high-temperature part of  $\xi(T)$ . In this range, the typical behavior is close to a power law  $T^{-\alpha}$ , which generates a power law shape  $E^{-\delta}$  in the corresponding high-energy part of  $\bar{F}(E)$  (the approximate relation  $\alpha \approx \delta + 1/2$  has been already discussed in Section 3.1). In this case, the small  $y$  (high  $T$ ) boundary condition (15) plays a constructive role in the recovery of  $\xi(T)$  and makes first-order regularization more effective than the projected iterative scheme (in this case, the action of the positivity constraint is insignificant, since the  $\xi(T)$  to be recovered has a wide support *i.e.* is everywhere far from zero and possible residual oscillations do not induce negative components). A test example is represented in Figure 4, where we invert the spectrum  $\bar{F}(E)$  corresponding to the input form

$$\xi(T) \approx T^{-5/2}. \quad (28)$$

This electron spectrum has been obtained by inverting the corresponding photon spectrum given by Equation (6) with the addition of realistic Poisson noise.  $\bar{F}(E)$  in Figure 4(a) has been uniformly sampled with  $N = 140$  points in the range 50–189 keV (in the case of power laws the sensitivity of the reconstruction qualities on the energy range adopted for the inversion is not very significant) and inverted in Figure 4(b) by means of the first-order regularization method and for the projected-Landweber method. The results of this computation clearly show that first-order regularization with the boundary condition (15) is particularly effective in this case. We finally note that for notably larger values of  $\delta$  a certain deterioration of the reconstructions may occur, due to the fact that  $\lambda$  is a global regularization parameter which works in a less effective way when the function to reconstruct

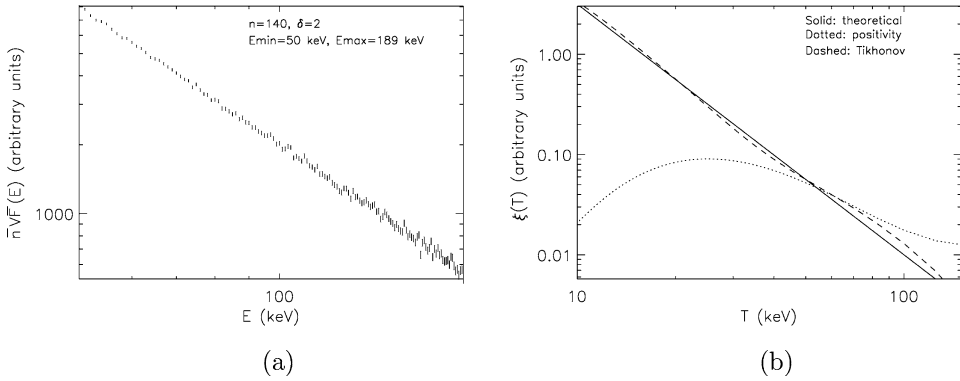


Figure 4. Inversion of  $\bar{F}(E)$  corresponding to the case  $\xi(T) \approx T^{-5/2}$ : (a)  $\bar{F}(E)$  uniformly sampled with  $N = 140$  points in the energy range 50 – 189 keV; (b) theoretical  $\xi(T)$  (*solid*), reconstruction given by first-order regularization (*dashed*), reconstruction given by the projected-Landweber method (*dotted*).

is steep. However, this deterioration can be reduced by means of an appropriate rescaling of the power law (see Kontar *et al.*, 2005).

### 3.4. MORE REALISTIC SPECTRA

A mean electron flux spectrum reconstructed from a real photon spectrum is often assumed (Holman *et al.*, 2003) to comprise an isothermal component at low electron energies plus a power law behavior at high energies. A simple example is given by the model electron spectrum (with  $T, E$  in keV)

$$\bar{F}(E) = 100 T_0^{-3/2} E e^{-\frac{E}{T_0}} + \frac{\Gamma(\delta + 1)}{100} \left(\frac{E}{50}\right)^{-\delta}; \quad (29)$$

application of the derivative test (Brown and Emslie, 1988) shows that this spectrum is consistent with a wholly thermal source; indeed the corresponding differential emission measure is

$$\xi(T) = 100 \delta (T - T_0) + 0.5(50)^{\delta-1} T^{-(\delta+0.5)}. \quad (30)$$

We discretized the  $\bar{F}(E)$  form (29) with a uniform one keV sampling from 1 to 250 keV with  $T_0 = 4$  keV and  $\delta = 2$ . We then generated the corresponding photon spectrum ( $I(\epsilon)$ ) using an exact (isotropic) cross-section and added random Poisson noise, resulting in corresponding noise in  $\bar{F}(E)$ . Figure 5(a) shows the resulting simulated  $\bar{F}(E)$ , while Figure 5(b) contains the restorations provided by the two methods. Both reconstructions present notable unphysical artefacts, which are essentially due to the fact that neither method is able to fully restore the two completely different behaviors of the source function at low and high  $T$ . Therefore, we considered an approach whereby the two different inversion methods are applied one to the low-energy and one to the high-energy part of the electron spectrum separately. More precisely, the projected-Landweber method is applied to  $\bar{F}(E)$  in the low-energy range (here we used 2–36 keV, which approximately corresponds to the range where the spectrum is optimally fitted by the isothermal component). On the other hand, first-order Tikhonov regularization with boundary conditions is applied to  $\bar{F}(E)$  in the high-energy range (here we used 55–204 keV, which approximately corresponds to the range where the spectrum is optimally fitted by a power law). The two reconstructed  $\xi(T)$  are connected together at the temperature where the thermal peak goes to zero, and it is plotted in Figure 5(c), while Figure 5(d) shows that the regularized cumulative residuals (24) are statistically reliable for the chosen value of the iteration number and of the Tikhonov regularization parameter.

## 4. Application to RHESSI Data

In order to address the analysis of real spectra provided by RHESSI, we first need to check the compatibility between condition (15) and the asymptotic behavior of

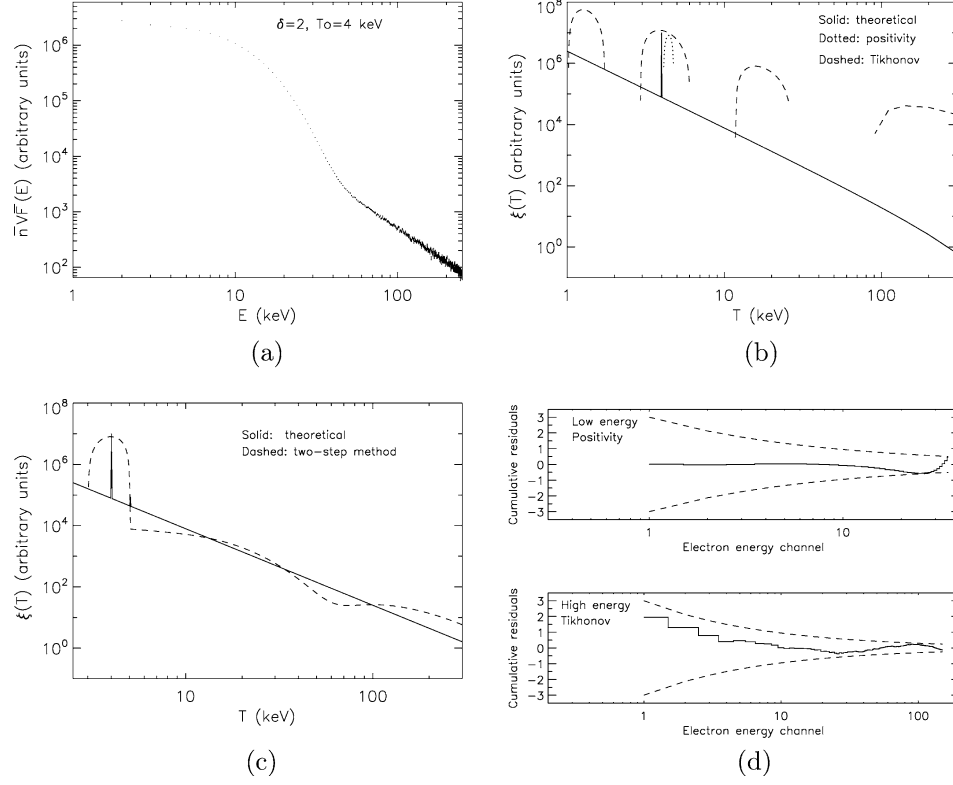


Figure 5. Inversion of  $\bar{F}(E)$  corresponding to  $\xi(T)$  given in Equation (30) for  $T_0 = 4$  keV and  $\delta = 2$ : (a) electron spectrum with  $N = 250$  sampled energies in the range 1–250 keV; (b) theoretical  $\xi(T)$  (solid) with the reconstructions given by first-order regularization (dashed) and projected-Landweber method (dotted); (c) theoretical  $\xi(T)$  (solid) and reconstruction (dashed) obtained by inverting the low-energy part of the electron spectrum with the projected-Landweber method and the high-energy part with first-order Tikhonov regularization and by connecting the two restorations; (d) cumulative regularized residuals (solid) for the method with positivity (upper panel) and Tikhonov regularization (lower panel) compared to the statistical bound  $\pm 3/\sqrt{k}$  (dashed).

the recorded photon spectrum at high energies. Such an issue can be addressed by simple integral computations showing that, if a function  $F(t)$ , for  $t \rightarrow 0$ , is

$$F(t) \approx At^\beta \quad (31)$$

with  $\beta > -1$ , then its Laplace transform  $(\mathcal{L}F)(s)$ , for  $t \rightarrow \infty$ , is

$$(\mathcal{L}F)(s) \approx A \frac{\Gamma(\beta + 1)}{s^{\beta+1}}, \quad (32)$$

with

$$\Gamma(z) = \int_0^\infty e^{-t} t^{z-1} dt. \quad (33)$$

Therefore, condition (15) is compatible with the mean source electron spectrum with an asymptotic ( $E \rightarrow \infty$ ) electron spectral index  $\delta > 0$  (corresponding to a photon spectral index  $\gamma > 1$ ).

The reconstruction procedure described in Section 3.4 has been applied to three photon spectra observed by RHESSI corresponding to three different flares. Figure 6(a) shows the photon spectrum corresponding to the August 21, 2002 flare in the time interval 01:38:44–01:39:04 UT, while Figure 6(b) shows the corresponding averaged electron spectrum obtained by using zero-order Tikhonov regularization as described by Piana *et al.* (2003). The low-energy part of this spectrum (11–24 keV) has been inverted by means of the Landweber iterative scheme with positivity for  $10^5$  iterations, while the high-energy part (50–189 keV) has been inverted by using first-order Tikhonov regularization with boundary conditions (again the two

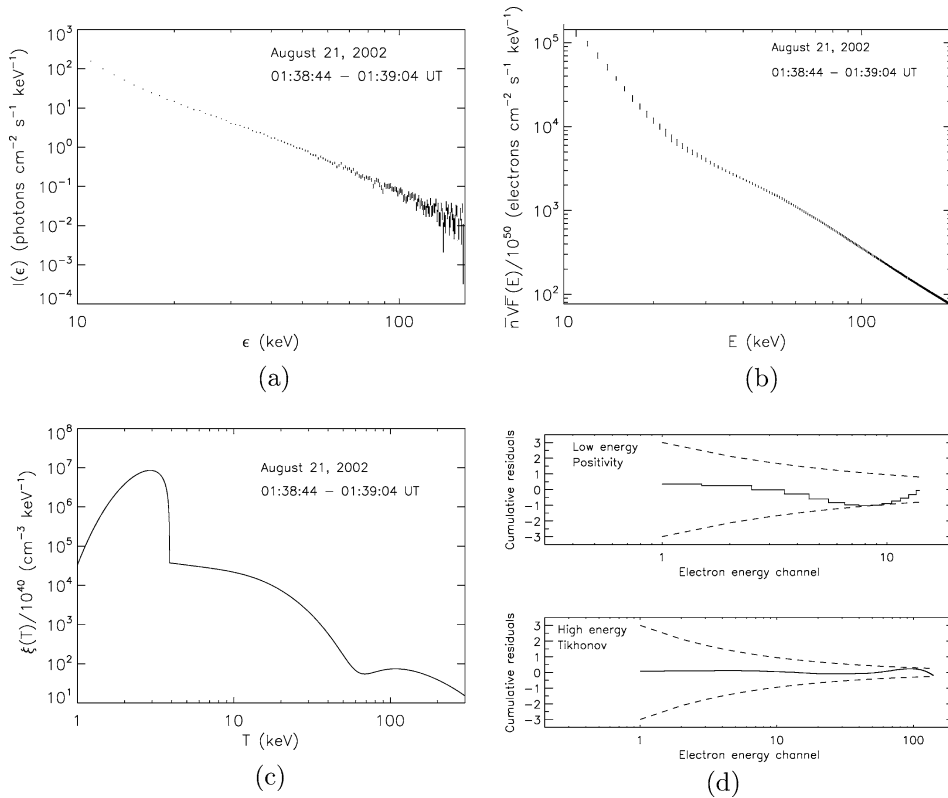


Figure 6. August 21, 2002 flare recorded by RHESSI in the time interval 01:38:44–01:39:04 UT: (a) photon spectrum; (b) mean source electron spectrum reconstructed by zero-order Tikhonov regularization; (c) reconstruction obtained by inverting the low-energy part of the electron spectrum with the projected-Landweber method and the high-energy part with first-order Tikhonov regularization and by connecting the two restorations; (d) cumulative regularized residuals (*solid*) for the method with positivity (*upper panel*) and Tikhonov regularization (*lower panel*) compared to the statistical bound  $\pm 3/\sqrt{k}$  (*dashed*).

electron energy ranges correspond to the intervals where  $\bar{F}(E)$  is optimally fitted by a thermal component and a power law respectively). The two reconstructed  $\xi(T)$  are connected together and plotted in Figure 6(c), while the cumulative residuals contained in Figure 6(d) show that the reconstruction is statistically reliable. At small  $T$ ,  $\xi(T)$  presents a peak at  $T \approx 2.9$  keV, FWHM  $\approx 1.5$  keV and  $\langle T \rangle \approx 2.8$  keV (the temperature provided by best-fitting  $\bar{F}(E)$  is 2.6 keV). In order to study the compatibility of this spectrum with a single-temperature thermal interpretation, we produced a synthetic  $\bar{F}(E)$  corresponding to a  $\delta$  function peaked at 2.9 keV and inverted it with the same projected-Landweber method applied to the same electron energy range. The restoration presented a FWHM of around 1.5 keV showing that this flare can be reliably interpreted according to an isothermal model. At higher temperatures,  $\xi(T)$  presents a dip between 60 and 70 keV and an asymptotic power law-like behavior with  $\alpha \approx 2.8$  (this value is in accordance with the fact that the asymptotic electron spectral index is  $\delta \approx 2.3$ ). In order to study the statistical relevance of the non-monotonic structure in the 60–70 keV temperature range, in Figure 7 we constructed the confidence strip for the regularized  $\xi(T)$  (Piana, 1994; Piana *et al.*, 2003) by means of repeated inversions using different realizations of the data set and by superimposing the corresponding regularized solutions. The strip results to be notably large in correspondence with the dip, thus allowing to interpret this structure in terms of a ‘plateau’, a broken-power-law or even a simple power law behavior.

An analogous procedure has been applied for the analysis of the photon spectrum in the time interval 09:57:00–09:57:20 UT of the November 3, 2003 flare (see Figure 8(a) for the photon spectrum and Figure 8(b) for the inverted averaged electron spectrum).  $\bar{F}(E)$  has been inverted with the positivity method in the 13.5–40.5 keV range and with first-order regularization in the 56.5–180.5 keV range. The reconstructed  $\xi(T)$  in Figure 8(c) presents a peak at  $T \approx 3.1$  keV with

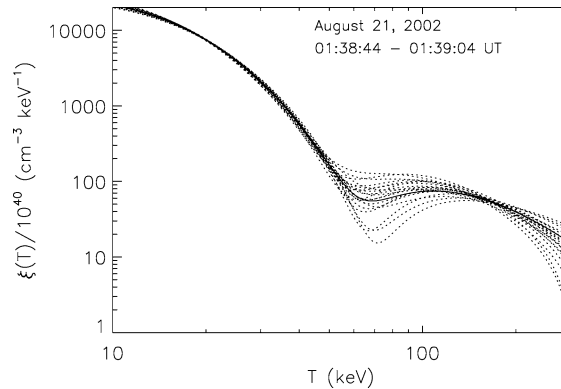


Figure 7. The confidence strip for the regularized  $\xi(T)$  at high  $T$ , corresponding to the August 21, 2002 flare in the time interval 01:38:44–01:39:04 UT. The strip has been obtained by repeated inversions of  $\bar{F}(E)$  in Figure 6(b) using 20 different random realizations of this data set. The inversion method is first-order Tikhonov regularization.

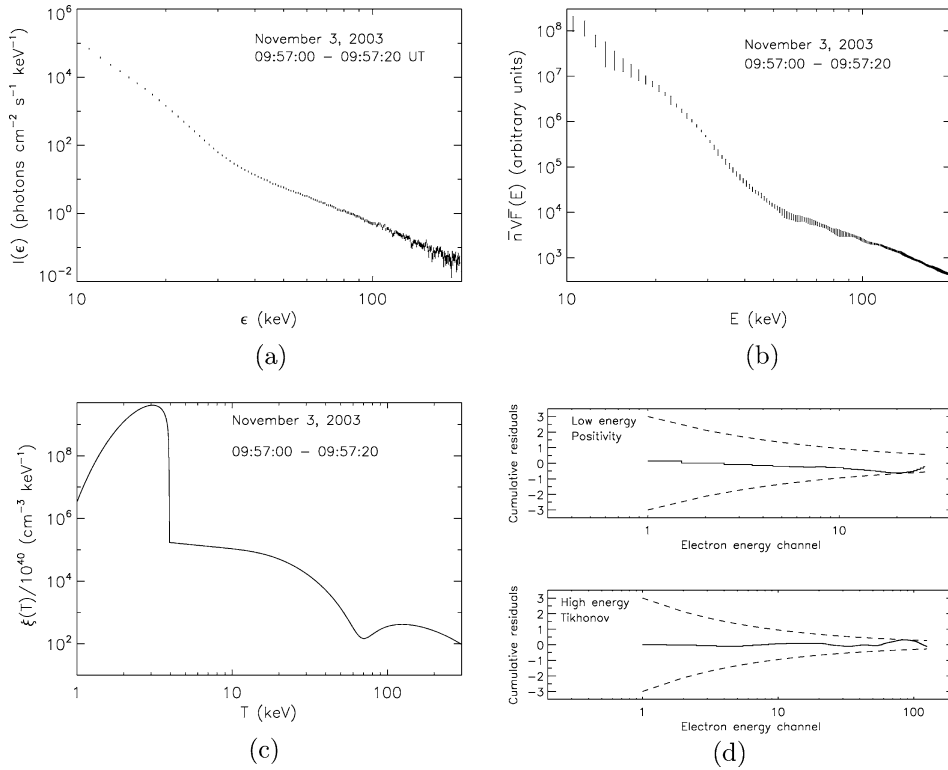


Figure 8. November 3, 2003 flare recorded by RHESSI in the time interval 09:57:00–09:57:20 UT: (a) photon spectrum; (b) mean source electron spectrum reconstructed by zero-order Tikhonov regularization; (c) reconstruction obtained by inverting the low-energy part of the electron spectrum with the projected-Landweber method and the high-energy part with first-order Tikhonov regularization and by connecting the two restorations; (d) cumulative regularized residuals (*solid*) for the method with positivity (*upper panel*) and Tikhonov regularization (*lower panel*) compared to the statistical bound  $\pm 3/\sqrt{k}$  (*dashed*).

$\text{FWHM} \approx 1.4 \text{ keV}$  and  $\langle T \rangle \approx 2.8 \text{ keV}$  (the best-fitting temperature is 3.2 keV). As for the previous flare, in this case, a single-temperature interpretation of this part of the spectrum is acceptable. At higher  $T$  there is a feature in the range 70 – 80 keV, which is more pronounced than the one in the August 21, 2002 flare (although, also in this case, the confidence strip at these temperatures is very wide). The asymptotic  $\alpha$  is around 3.1, which must be compared with an asymptotic  $\delta$  in  $\bar{F}(E)$  of around 2.7 (once more, the asymptotic relation  $\alpha \sim \delta + 0.5$  is satisfied). The cumulative residuals in Figure 8(d) show that these results are statistically reliable.

Things are notably different in the case of the photon and electron spectra in Figure 9(a) and (b), respectively, corresponding to the time interval 00:30:00–00:30:20 UT of the July 23, 2002 flare. This  $\bar{F}(E)$  fails the derivative test at several points in the low-energy range. We have computed the first five derivatives of

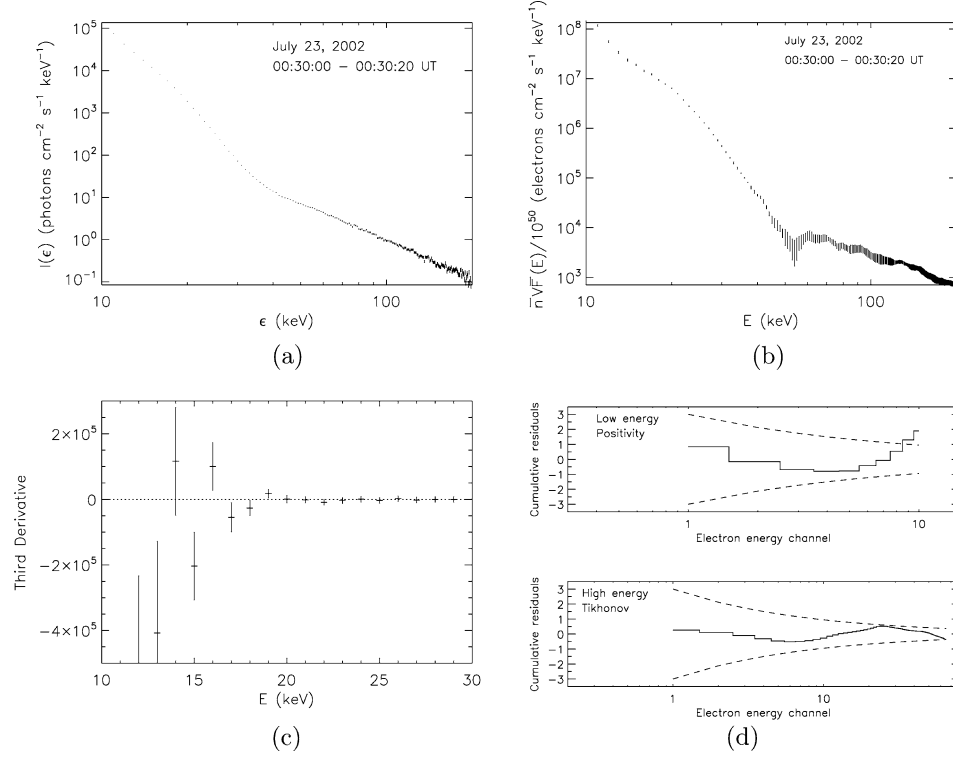


Figure 9. July 23, 2002 flare recorded by RHESSI in the time interval 00:30:00–00:30:20 UT: (a) photon spectrum; (b) mean source electron spectrum reconstructed by zero-order Tikhonov regularization; (c) numerical third derivative of  $\bar{F}(E)/E$  with corresponding statistical errors; (d) cumulative regularized residual (*solid*) for the method with positivity (*upper panel*) in the case of  $10^6$  iterations and Tikhonov regularization (*lower panel*) compared to the statistical bound  $\pm 3/\sqrt{k}$  (*dashed*).

$\bar{F}(E)/E$  and found failures of the test for different points in the second, third, fourth, and fifth derivative. Figure 9(c) contains, for example, the third derivative, which should be negative for a thermal spectrum, and which is in fact positive (with statistical significance) at 16 and 19 keV. By applying the constrained-Landweber method to  $\bar{F}(E)$  at low energies (for example between 12 and 21 keV) we found that the cumulative residuals never present the expected random walk, even for huge numbers of iterations (the residuals in Figure 9(d), upper panel, correspond to  $10^6$  iterations). This behavior seems to suggest that a thermal interpretation of this photon spectrum could be problematic, although we also observe that this photon data set probably suffers a notable pulse pile-up, which may imply artefacts in the reconstruction of  $\bar{F}(E)$ . For the high-energy part of the spectrum, first-order regularization provides a power law-like  $\xi(T)$  with  $\alpha \approx 2.7$  at high  $T$  ( $\delta$  for this spectrum is around 2).

## 5. Conclusions

The inference of differential emission measure functions ( $\xi(T)$ ) from observed photon spectra ( $I(\epsilon)$ ) with a realistic bremsstrahlung cross-section is substantially more difficult than the single-step inversion analysis of Piana, Brown, and Thompson (1995) based on an approximate  $Q$ . A proper procedure involves two inverse problems. The first of these is the inversion of  $I(\epsilon)$ , through an exact solid-angle-averaged bremsstrahlung cross-section kernel and a zero-order Tikhonov regularization method, to obtain the mean source electron spectrum  $\bar{F}(E)$ . The second uses an approach for inverting  $\bar{F}(E)$ , which involves the application of a projected algorithm with positivity constraint in the inversion of the low-energy part of the spectrum and of a first-order regularization method with boundary conditions in the inversion of the high-energy part of the spectrum. The main findings are as follows:

- The approach correctly identifies certain properties of  $\bar{F}(E)$  (such as bumps or energy cutoffs) as being inconsistent with any physical  $\xi(T) \geq 0$ .
- The use of the positivity constraint allows us to obtain a satisfactory temperature resolution in the recovery of  $\delta$  functions, while the use of first-order regularization with boundary conditions provides reliable reconstructions for smooth forms such as power laws.
- Application of the method to observed RHESSI photon spectra has revealed two cases in which the recovered  $\xi(T)$  is spectrally consistent with a roughly isothermal low-temperature plasma plus a very broad form of  $\xi(T)$  at high temperatures. In a third case, a spectrum from the July 23, 2002 flare, the reconstruction method at low temperatures produces unacceptable large residuals. This result is in accordance with the fact that the same spectrum fails to satisfy the derivative test, which verifies the compatibility with a purely thermal interpretation. Possible physical motivations for this behavior are still unclear and, for example, may be related to the fact that this flare produced spectra which deviate from a power law behavior in a manner consistent with nonuniform ionization (Kontar *et al.*, 2003). However, we also observe that the spectrum used in our analysis suffers a notable pulse pile-up, which may imply artefacts in the analysis results.

The availability of a reconstruction approach for addressing the difficult inverse problem of restoring  $\xi(T)$  from reconstructions of  $\bar{F}(E)$  may have important consequences in the analysis and interpretation of RHESSI spectra. In future research, we will apply the method to study the influence of albedo effects on the modification of the differential emission measure and to deduce important physical properties on the thermal plasma from the reconstructed  $\xi(T)$ .

### Acknowledgements

This work has been partially supported by a grant of the Italian GNCS-INdAM, by Italian MIUR, by a grant of the Swiss International Space Science Institute (ISSI) and by a UK PPARC Rolling Grant (JCB, EPK). AGE was supported by NASA's Office of Space Science.

### References

- Bertero, M.: 1989, in P.W. Hawkes (ed.), *Advances in Electronics and Electron Physics* **75**, Academic Press, New York, p. 1.
- Bertero, M., Brianzi, P., and Pike, E.R.: 1982, *Proc. R. Soc. Lond. Ser. A* **383**, 15.
- Bertero, M., Brianzi, P., and Pike, E.R.: 1985, *Inverse Problems* **1**, 1.
- Brianzi, P. and Frontini, M.: 1991, *Inverse Problems* **7**, 355.
- Brown, J.C.: 1971, *Solar Phys.* **18**, 489.
- Brown, J.C.: 1974, in G.A. Newkirk (ed.) *Coronal Disturbances I.A.U. Symp.* **57**, Surfers Paradise, p. 395.
- Brown, J.C. and Emslie, A.G.: 1988, *Astrophys. J.* **331**, 554.
- Brown, J.C., Emslie, A.G., and Kontar, E.P.: 2003, *Astrophys. J.* **595**, L115.
- Brown, J.C., Melrose, D.B., and Spicer, D.S.: 1979, *Astrophys. J.* **228**, 592.
- Craig, I.J.D. and Brown, J.C.: 1986, *Inverse Problems in Astronomy*, Adam Hilger, New York.
- Davies, A.M.: 1992, in M. Bertero and E.R. Pike (eds.), *Inverse Problems in Scattering and Imaging*, Adam Hilger, Bristol, p. 393.
- Davies, B. and Martin, B.: 1979, *J. Comput. Phys.* **33**, 1.
- Eicke, B.: 1992, *Numer. Funct. Anal. Opt.* **13**, 413.
- Emslie, A.G., Coffey, V.N., and Schwartz, R.A.: 1989, *Solar Phys.* **122**, 313.
- Essah, W.A. and Delves, L.M.: 1988, *Inverse Problems* **4**, 705.
- Gabriel, A.H.: 1992, in J. Schmelz and J.C. Brown (eds.), *The Sun: a Laboratory for Astrophysics*, NATO ASI, Kluwer Academic Publishers, Dordrecht, p. 423.
- Golub, G. and van Loan, C.: 1996, *Matrix Computations*, Johns Hopkins, London.
- Holman, G.D., Sui, L., Schwartz, R.A., and Emslie, A.G.: 2003, *Astrophys. J.* **595**, L97.
- Johns, C.M. and Lin, R.P.: 1992, *Solar Phys.* **137**, 121.
- Kato, T.: 1980, *Perturbation Theory for Linear Operators*, Springer, Berlin.
- Koch, H.W. and Motz, J.W.: 1959, *Rev. Mod. Phys.* **31**, 920.
- Kontar, E.P., Brown, J.C., Emslie, A.G., Schwartz, R.A., Smith, D.M., and Alexander, R.C.: 2003, *Astrophys. J.* **595**, L123.
- Kontar, E.P., Emslie, A.G., Piana, M., Massone, A.M., and Brown, J.C.: 2005, *Solar Phys.* **226**, 317.
- Kontar, E.P., Piana, M., Massone, A.M., Emslie, A.G., and Brown, J.C.: 2004, *Solar Phys.* **225**, 293.
- Korchak, A.A. and Ponomarenko, Y.B.: 1965, *Geomagn. Aeron.* **6**, 417.
- Kress, R.: 1989, *Linear Integral Equations*, Springer, Berlin.
- Legendijk, R., Biemond, J., and Boeckee, D.: 1988, *IEEE Trans. Acoust. Speech Signal Proc.* **36**, 1874.
- Lin, R.P. and Schwartz, R.A.: 1987, *Astrophys. J.* **312**, 462.
- Lin, R.P., et al.: 2002, *Solar Phys.* **210**, 3.
- Massone, A.M., Piana, M., Conway, A.J., and Eves, B.: 2003, *Astron. Astrophys.* **405**, 325.
- McWhirter, J.G. and Pike, E.R.: 1978, *J. Phys. A* **11**, 1729.
- Piana, M.: 1994, *Astron. Astrophys.* **288**, 949.

- Piana, M. and Bertero, M.: 1996, *J. Opt. Soc. Am. A* **13**, 1516.
- Piana, M. and Bertero, M.: 1997, *Inverse Problems* **13**, 441.
- Piana, M. and Brown, J.C.: 1998, *Astron. Astrophys.* **132**, 291.
- Piana, M., Brown, J.C., and Thompson, A.M.: 1995, *Solar Phys.* **156**, 315.
- Piana, M., Massone, A.M., Kontar, E.P., Emslie, A.G., Brown, J.C., and Schwartz, R.A.: 2003, *Astrophys. J.* **595**, L127.
- Thompson, A.M., Brown, J.C., Craig, I.J.D., and Fulber, C.: 1992, *Astron. Astrophys.* **265**, 278.
- Tikhonov, A.N.: 1963, *Sov. Math. Dokl.* **4**, 1035.
- Varah, J.M.: 1983, *SIAM J. Sci. Stat. Comput.* **4**, 164.